

A radial velocity survey for post-common-envelope Wolf-Rayet central stars of planetary nebulae: First results and discovery of the close binary nucleus of NGC 5189*

Rajeev Manick,^{1,2,3†} Brent Miszalski^{1,4} and Vanessa McBride^{1,2}

¹South African Astronomical Observatory, PO Box 9, Observatory, 7935, South Africa

²Astrophysics, Cosmology and Gravity Centre, Department of Astronomy, University of Cape Town, Private Bag X3, Rondebosch 7701, South Africa

³Instituut voor Sterrenkunde, KU Leuven, Celestijnenlaan 200D bus 2401, B-3001 Leuven, Belgium

⁴Southern African Large Telescope Foundation, PO Box 9, Observatory, 7935, South Africa

Accepted Received ; in original form

ABSTRACT

The formation of Wolf-Rayet central stars of planetary nebulae ([WR] CSPNe) whose spectroscopic appearance mimics massive WR stars remains poorly understood. Least understood is the nature and frequency of binary companions to [WR] CSPNe that may explain their H-deficiency. We have conducted a systematic radial velocity (RV) study of 6 [WR] CSPNe to search for post-common-envelope (post-CE) [WR] binaries. We used a cross-correlation method to construct the RV time-series as successfully done for massive close binary WR stars. No significant RV variability was detected for the late-[WC] type nuclei of Hen 2-113, Hen 3-1333, PMR 2 and Hen 2-99. Significant, large-amplitude variability was found in the [WC4] nucleus of NGC 5315. In the [WO1] nucleus of NGC 5189 we discovered significant periodic variability that reveals a close binary with $P_{\text{orb}} = 4.04 \pm 0.1$ d. We measured a semi-amplitude of 62.3 ± 1.3 km s⁻¹ that gives a companion mass of $m_2 \geq 0.5 M_{\odot}$ or $m_2 = 0.84 M_{\odot}$ (assuming $i = 45^\circ$). The most plausible companion type is a massive WD as found in Fleming 1. The spectacular nebular morphology of NGC 5189 fits the pattern of recently discovered post-CE PNe extremely well with its dominant low-ionisation structures (e.g. as in NGC 6326) and collimated outflows (e.g. as in Fleming 1). The anomalously long 4.04 d orbital period is either a once-off (e.g. NGC 2346) or it may indicate there is a sizeable population of [WR] binaries with massive WD companions in relatively wide orbits, perhaps influenced by interactions with the strong [WR] wind.

Key words: planetary nebulae: general - stars: Wolf-Rayet - stars: AGB and post-AGB - planetary nebulae: individual: NGC 5189 - binaries: spectroscopic

1 INTRODUCTION

Planetary nebulae (PNe) are circumstellar gas envelopes ejected at the end of the Asymptotic Giant Branch (AGB) phase of low-intermediate mass stars of $\sim 1M_{\odot}$ to $8M_{\odot}$. A majority of central stars of planetary nebulae (CSPNe) show hydrogen rich atmospheres (e.g. Méndez et al. 1988; Méndez 1991; Napiwotzki & Schoenberner 1995), with their spectra containing only weak absorption lines, mainly of hydrogen

(H) and helium (He). Perhaps the least understood are the less numerous emission-line CSPNe with H-deficient atmospheres whose spectral appearance mimics the massive Wolf-Rayet (WR) stars. These CSPNe exhibit dense and strong stellar winds with mass-loss rates up to $\sim 10^{-7} M_{\odot} \text{ yr}^{-1}$ (e.g. Koesterke 2001; Crowther 2008). Their classification is similar to massive WR stars where the dominant emission lines indicate either a [WC] (He, C and O; Crowther et al. 1998) or [WN] (He and N; Smith et al. 1996) subtype, where the brackets around the spectral type distinguish them from their massive counterparts. In contrast to the roughly equal division between WN and WC subtypes in massive WR stars (van der Hucht 2001), the known examples of [WR] stars are heavily skewed towards early and late [WC] types with few

* Based on observations made with the South African Astronomical Observatory (SAAO) 1.9-m telescope and the Southern African Large Telescope (SALT) under programme 2013-2-RSA-005 (PI: Miszalski).
† E-mail: rajeev@ster.kuleuven.be

intermediate [WC] types (Crowther 2008; see however Górny 2014), whereas only two bona-fide [WN] CSPNe were established recently in IC 4663 (Miszalski et al. 2012) and A 48 (Todt et al. 2013; Frew et al. 2014). Comprehending this disparity may shed much needed light on how [WR] stars form.

The most peculiar aspect of the newly discovered [WN] CSPNe is that their atmospheres are extremely helium rich (85–95 per cent by mass, Miszalski et al. 2012; Todt et al. 2013). Therefore, they do not fit into the C-rich evolutionary sequence that the vast majority of H-deficient post-AGB stars follow (Werner & Herwig 2006). The C-rich H-deficient post-AGB evolutionary sequence of [WC] stars evolving into PG1159 stars, the latter characterised by significantly weaker winds and higher surface gravities, is well supported by similar atmospheric abundance patterns between the two classes (Crowther 2008; Werner et al. 2008). Werner (2012) suggested that [WN] CSPNe ‘might’ be the progenitors of O(He) stars, namely a rare group of four high surface gravity He-rich post-AGB stars, two of which are surrounded by PNe (Rauch et al. 1994, 1996, 1998, 2008; Reindl et al. 2013, 2014). However, the existence of [WN] CSPNe was still unproven at this time and PB 8 was not He-rich enough to be strictly comparable to the O(He) stars. Only with the discovery of the extremely He-rich atmosphere of the [WN3] CSPN of IC 4663 (95 per cent He by mass) could the O(He) stars, which are similarly He-rich with He mass fractions $\gtrsim 90$ per cent (Reindl et al. 2013, 2014), be securely linked to [WN] CSPNe in a separate He-rich H-deficient post-AGB evolutionary sequence [WN]→O(He) by Miszalski et al. (2012). In this new sequence the O(He) stars are the He-rich analogues of the C-rich PG1159 stars.

A key question prompted by the discovery of the He-rich sequence is whether it operates in a similar fashion to the C-rich sequence. Is the appearance of the [WR] phenomenon produced by the same recipe? Or is the phenomenon produced via separate routes with different recipes? There are compelling arguments to include binary interactions in the formation of some [WC] CSPNe and related objects (De Marco & Soker 2002; De Marco 2008) for which the standard formation scenarios of a late thermal pulse (LTP) (e.g. Schoenberner 1979; Blöcker 2001; Herwig 2001), a very late thermal pulse (VLTP) (e.g. Lawlor & MacDonald 2002), or an AGB final thermal pulse (AFTP) (e.g. Herwig 2001) may not apply.¹ Miszalski et al. (2012) suggested a merger may be responsible for the high He enrichment in IC 4663 and Reindl et al. (2013) found a reasonable agreement between the atmospheric composition of IC 4663 and that predicted from a slow merger of two He-WDs (Zhang & Jeffery 2012). A merger scenario would be consistent with the extreme rar-

ity of both [WN] and O(He) stars compared to their C-rich counterparts, however it may not be possible to prove observationally. Some other scenarios were discussed by Reindl et al. (2014), however we emphasise that many of the scenarios require considerably more theoretical and, in particular, observational investigation.

Unfortunately, there is currently insufficient evidence to gauge whether binary interactions in H-deficient post-AGB stars are widespread. Are the known binaries merely an oddity where the [WR] component formed independently of binary evolution? Or was a binary interaction fundamental to forming the [WR] component?

Several different possibilities for binary interactions were proposed by De Marco & Soker (2002) and De Marco (2008), however the paucity of observed binary systems makes it difficult to discern to what degree these or some other scenarios may play a role. In this work we aim to address this by searching for companions in a sample of [WR] central stars. It is more practical with modest amounts of telescope time to search for close binaries where the orbital periods are a few days or less, signifying that a common-envelope (CE) interaction has produced the observed short orbital periods (Iben & Livio 1993; Ivanova et al. 2013). Only two previous post-CE examples have been discovered, namely SDSS J212531.92–010745.9 that consists of a PG1159 star with an M dwarf companion (Nagel et al. 2006; Schuh et al. 2009) and the [WC7] CSPN of PN G222.8–04.2 with an undetermined companion type (Hajduk et al. 2010). Their literature orbital periods are 0.29 d and 0.63 or 1.26 d, respectively.

The majority of close binary CSPNe have been found via photometry monitoring including PN G222.8–04.2.² There are however several limitations with this approach. A notable exception is the double degenerate nucleus of Fleming 1 (Boffin et al. 2012), discovered from radial velocity (RV) monitoring. The companion in Fleming 1 is a more massive WD whose presence is not detectable in the optical lightcurve. At least 37 unique early-type [WC], PG 1159 and O(He) CSPNe have been subjected to photometric monitoring campaigns to search for non-radial pulsations (Ciardullo & Bond 1996; Gonzalez-Perez et al. 2006), however no close binaries have been discovered as part of these campaigns. If ~ 15 –20 per cent of PNe are expected to host close binaries (Bond 2000; Miszalski et al. 2009a), then we would have expected ~ 5 –7 close binaries amongst the sample. It is particularly suprising that no binaries were found, especially since they are amongst the hottest CSPNe known and as such they would have produced a very large irradiation effect if a close main sequence companion was present (e.g. Corradi et al. 2011; Miszalski et al. 2011). If these CSPNe were to have companions, they are most likely evolved, massive WD companions as in Fleming 1 (Boffin et al. 2012). Another possibility is that there are main sequence companions present with orbital periods of several days or months, for which an irradiation effect would not be detected (e.g. De Marco et al. 2008). An RV monitoring study is therefore the least biased method to search for elusive [WR] close binary CSPNe, however such a study has not been previously attempted. Previously researchers have focused primarily on

¹ These scenarios cannot reproduce the moderate level of ~ 55 per cent He by mass in the possible intermediate [WN/WC] CSPN of PB 8 (Todt et al. 2010). Miller Bertolami et al. (2011) proposed a diffusion induced nova scenario to explain the abundance pattern of PB 8, however these models require low metallicities and core masses to reach the extremely He-rich compositions of [WN] CSPNe (see the discussion in Todt et al. 2013). While it seems that low metallicities may facilitate [WR] formation (Zijlstra et al. 2006; Kniazev et al. 2008), the α -element nebular abundances of both IC4663 and A 48 are notably Solar, suggesting the Miller Bertolami et al. (2011) scenario may not be applicable.

² See Table A1 in Appendix for an updated compilation.

Of-type CSPNe, whose photometry (e.g. Handler 2003) and line profiles (e.g. Méndez 1990; De Marco et al. 2004; De Marco 2009) show significant variability. Perhaps one reason these studies have not been extended to [WR] CSPNe is that they were presumed to be similarly affected by wind variability (if not more so for those with faster wind speeds), however several studies of massive WR stars have routinely found close binaries (Foellmi et al. 2003; Sana et al. 2013; Schnurr 2008; Schnurr et al. 2009) and there is no reason to suspect the same methods cannot be applied to [WR] CSPNe.

This paper is structured as follows: Section 2 describes our sample selection and the observations. Section 3 gives an overview of the cross-correlation method used to find RV shifts in the spectra. In Section 4 we present our results for each object and we perform a χ^2 analysis to quantify variability. Section 5 derives the orbital period and mass function of the most variable object, NGC 5189, before discussing the nature of the companion and the nebular morphology. We conclude in Section 6.

2 OBSERVATIONS

2.1 Sample selection

Table 1 gives the basic properties of the objects considered in this pilot study. All were monitored using the cassegrain spectrograph (SpCCD) on the South African Astronomical Observatory (SAAO) 1.9-m telescope except for NGC 5189 which was observed with the Robert Stobie Spectrograph (RSS; Burgh et al. 2003; Kobulnicky et al. 2003) on the queue-scheduled Southern African Large Telescope (SALT; Buckley, Swart & Meiring 2006; O’Donoghue et al. 2006). In general we required the spectra to have a resolution of $\lesssim 2\text{\AA}$ (full-width at half maximum, FWHM) and $S/N \gtrsim 40$ in the continuum to be able to ensure cross-correlation techniques could achieve a velocity accuracy of $\sim 10 \text{ km s}^{-1}$ or better. Given the relatively poor throughput of SpCCD, we were heavily restricted in our choice of [WR] CSPNe to monitor, namely those brighter than $V \lesssim 14$ mag. Therefore we selected several suitably bright targets visible at the time of observations from Acker & Neiner (2003) and one from Morgan et al. (2001). The magnitude restrictions also imposed a bias towards intrinsically brighter late [WC] CSPNe. The sample observed by the SAAO 1.9-m is not particularly remarkable, apart from the peculiar morphologies of Hen 2-113 (Lagadec et al. 2006) and Hen 3-1333 (Chesneau et al. 2006). Both Hen 2-113 and Hen 3-1333 exhibit dual-dust chemistry which may have originated from binary evolution. A binary system may be necessary to explain the resolved dust disk in Hen 3-1333 (De Marco et al. 2002; Chesneau et al. 2006) as they are a prevailing feature of post-AGB binaries (Van Winckel et al. 2009). The inclusion of NGC 5189 was specially motivated for SALT observations as described in the following.

NGC 5189 (PN G307.2–03.4) is a bright, remarkably peculiar southern PN that has long perplexed astronomers. It was discovered in 1826 by J. Dunlop from Australia (Cozens, Walsh & Orchiston 2010), but its unusual appearance meant that it was not until much later that it was recognised to be a PN with a ‘quasi-planetary’ classification assigned by

Henize (1967). The filamentary nebula has been described as ‘a graceful affair of recurvant gaseous draperies’ (Evans 1968) and its notorious complexity is the result of multiple point-symmetric low-ionisation knots or ansae (Phillips & Reay 1983; Hua, Dopita & Martinis 1998; Gonçalves et al. 2001; Sabin et al. 2012). Phillips & Reay (1983) suggested that the point-symmetric features were the result of precession due to a binary nucleus with an orbital period on the order of a few days. Unfortunately, since then no efforts have been made in the literature to determine if NGC 5189 has a close binary nucleus. The central star has a [WO1] spectral type (Crowther et al. 1998) and is amongst the hottest of all central stars at $165_{-8}^{+18} \text{ kK}$ (Keller et al. 2014). Ciardullo & Bond (1996) monitored the central star for ~ 9 hours and found a low-amplitude pulsation period of $11.51 \pm 0.05 \text{ min}$ that is typical of stars of its ilk (Ciardullo & Bond 1996; Gonzalez-Perez et al. 1996), but noted no other variability that might otherwise indicate a companion is present.

2.2 SAAO 1.9-m spectroscopy

Table 2 gives a summary of the observations with the SpCCD spectrograph on the SAAO 1.9-m. They were conducted over two separate weeks namely May 16 to 23 of 2012 and June 26 to 4 of 2012. We use the modified julian date (MJD=JD-2400000.5) as the time of the middle of each exposure. A slit width of $1.5''$ was used. Both grating 4 (1200 lines mm^{-1}) and 6 (600 lines mm^{-1}) were used in the observing runs. A dispersion of 0.49 and 1.09 $\text{\AA}/\text{pix}$ for the high resolution and low resolution spectra were obtained, respectively. The wavelength coverage of grating 4 is 855 \AA at $\sim 1.09 \text{\AA}$ resolution (FWHM) and 1840 \AA at $\sim 2.4 \text{\AA}$ resolution (FWHM) for grating 6. The CCD was read out with a binning factor of 1×2 in dispersion and spatial axes, respectively. A Copper Argon (CuAr) arc lamp was taken before and after each exposure to calibrate the wavelength scale. Both short ($\sim 240\text{s}$) and long exposures ($\sim 2400\text{s}$) were taken for each target, since we needed both unsaturated nebular emission lines and deep enough exposures to reach a S/N of $> 30 - 40$ in the continuum. The S/N was measured as an average of 4 different S/N at wavelengths $\sim 4220 \text{\AA}$, 4755 \AA , 5290 \AA and 5620 \AA for the blue spectra and $\sim 5990 \text{\AA}$, 6415 \AA , 6950 \AA and 7370 \AA for the red. The mean spectral resolution varied from 2.5 \AA to 2.9 \AA . The observations were mostly made when the seeing ranged between $\sim 1.5''$ to $2.5''$. The wavelength range was chosen according to the moon phase (blue wavelengths for grey/dark and red wavelengths for bright).

The 2D frames were trimmed and the overscan region bias level was subtracted. The L.A. Cosmic (van Dokkum 2001) IRAF task was used to cosmic-ray-clean the images. Wavelength calibration was performed in the standard fashion and the mean rms achieved in the IRAF task IDENTIFY was ~ 0.09 and ~ 0.15 for high and low resolution spectra, respectively. Each solution was applied to the appropriate object spectrum by adding the FITS header keywords REFSPEC1 and REFSPEC2 in the header of the object and processing them with the IRAF task DISPCOR. The two arcs were interpolated for the final solution, in case there was any small shift in the arc during the exposure (e.g. due to influence of gravity on the grating causing flexure). We did not find evidence of any substantial shift in the arcs. One-

Table 1. Basic properties of the sample of [WR] CSPNe observed.

PNG	Name	RA	Dec.	V	Type	Epochs	Ref.
291.3+08.4	PMR 2	11 34 38.6	−52 43 33	13.3	[WC9/10]	7	c
307.2−03.4	NGC 5189	13 33 32.8	−65 58 27	14.5	[WO1]	14	b,d
309.0−04.2	Hen 2-99	13 52 30.7	−66 23 26	13.3	[WC9]	7	a,b
309.1−04.3	NGC 5315	13 53 57.1	−66 30 51	14.4	[WC4]	4	a,b
321.0+03.9	Hen 2-113	14 59 53.5	−54 18 07	11.9	[WC10]	12	a,b
332.9−09.9	Hen 3-1333	17 09 00.9	−56 54 48	10.9	[WC10]	7	a,b

References: (a): Acker and Neiner (2003). (b): Crowther et al. (1998). (c): Morgan et. al. (2001). (d): Ciardullo et al. (1999).

dimensional spectra were extracted using the APALL task. The CSPN was extracted, subtracting the immediate nebular background (4 pixels either side). However, for late [WC] types this becomes difficult due to a lack of clearly-defined nebular emission lines.

2.3 SALT RSS spectroscopy

We obtained 14 RSS spectra of NGC 5189 with the queue-scheduled SALT under programme 2013-2-RSA-005 (PI: Miszalski). Table 2 includes the log of observations taken during January to March 2014. The PG2300 grating was used at a camera articulation angle of 70 deg to cover $\lambda = 4442\text{--}5462\text{ \AA}$ which contains several of the highest ionisation emission lines from the CSPN of NGC 5189 (e.g. O VI, N V, He II) which are formed in the wind closer to the [WO] star than lower ionisation species would (e.g. in later type [WC] stars), thereby improving the chances of detecting orbital motion (see e.g. Sana et al. 2013). The 1.5 arcsec wide slit was used at a position angle of 90 deg and resulted in a mean resolution of 2.1 \AA (FWHM) and a mean dispersion of 0.32 \AA/pix . The S/N was measured as an average of 4 different S/N at wavelengths $\sim 4580\text{ \AA}$, 4770 \AA , 5040 \AA and 5225 \AA for all spectra. A ThAr arc lamp exposure was taken before and after each science exposure. Basic reductions were applied using the PYSALT³ package (Crawford et al. 2010) and cosmic ray events were cleaned using the LACOSMIC package (van Dokkum 2001). Wavelength calibration was performed using standard IRAF tasks IDENTIFY, REIDENTIFY, FITCOORDS and TRANSFORM by identifying the arc lines in each row and applying a geometric transformation to the data frames. Both the before and after arc exposures were used to derive the fit for the geometric transformation and the resulting wavelength solution for all spectra had an RMS of $0.06 \pm 0.02\text{ \AA}$. One-dimensional spectra were extracted using the APALL task, namely a main extraction of the CSPN where the immediate nebular background (10 pixels on either side corresponding to 5.1 arcsec) was subtracted and a second extraction of the nebula where the subtracted background was taken from outside the nebula (15 pixels on one side only corresponding to 7.6 arcsec) to permit measurement of nebular radial velocities close to the CSPN position. No flux calibration was performed as the spectra were normalised for the cross-correlation analysis (see Figure 2).

In Figures 1 and 2 we show representative spectra of each object split over the whole wavelength range. The strongest over-subtracted nebular lines in the spectra of NGC 5189 have been interpolated over.

3 METHOD

3.1 Cross-correlation method & template construction

The method used for finding radial velocity (RV) shifts in the spectra is cross-correlation as described by Foellmi et al. (2003). The cross-correlation task used is XCSAO found in the RVSAO package (Kurtz & Mink 1998) that is executed in the IRAF environment. XCSAO multiplies the Fourier Transform (FT) of the object spectrum with the conjugate of the transform of a high S/N ratio zero-velocity template. For a detailed overview of the cross-correlation analysis, see Tonry & Davis (1979). This method has proved to be very useful in finding RV shifts in close massive WR binaries (Foellmi et al. 2003; Sana et al. 2013; Schnurr 2008; Schnurr et al. 2009). Despite the strong winds in [WR] CSPNe, this method is still applicable for finding binaries in these systems.

For a consistent RV monitoring programme, the cross-correlation template must have high S/N in the continuum. The object spectra need to be cross-correlated with this high SNR zero-velocity template to obtain accurate RV shifts. After having applied a heliocentric correction to the radial velocities using the BCVCORR package in IRAF, the template was constructed. The main steps involved in creating the template is outlined as follows:

- (i) Normalise all spectra.
- (ii) Subtract unity from the continuum.
- (iii) Convert all spectra to a logarithmic wavelength scale.
- (iv) Use the spectrum which has the highest S/N in the continuum as first template (T1) for cross-correlation.
- (v) Use the output by XCSAO of the first cross-correlation results to shift all spectra to the same “zero-velocity” as the T1 template.
- (vi) Finally, combine all the shifted spectra to create a zero-velocity template (T2) using the IRAF task SCOMBINE providing greater weights to the spectra having higher S/N in the continuum.

Once the template T2 was built, the cross-correlation is run again on the spectra, but with T2 as the template. The spectral regions which contain most of the stellar lines (excluding the nebular emission lines as far as possible) were

³ <http://pysalt.salt.ac.za>

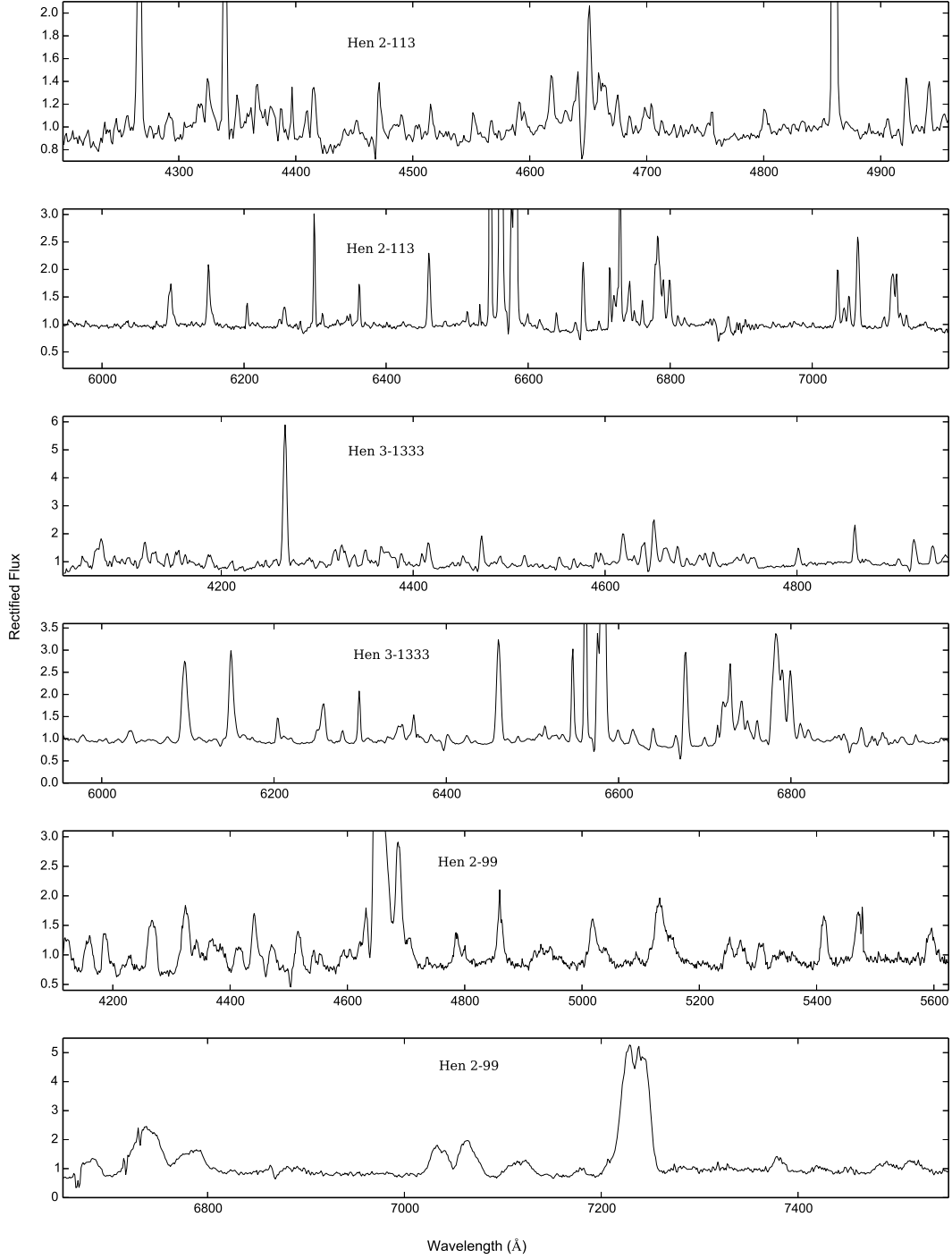


Figure 1. Representative spectra of objects in our sample.

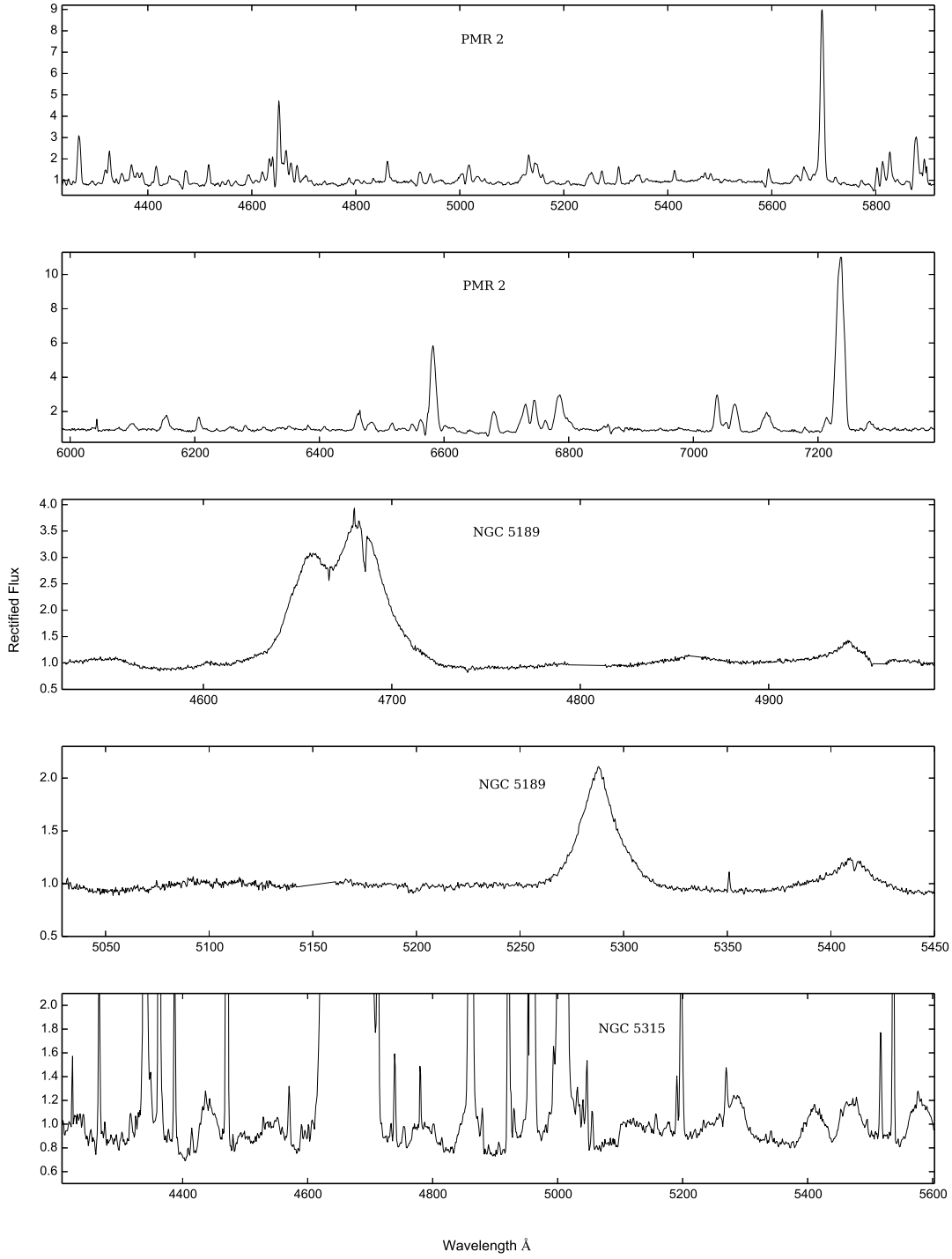


Figure 2. Figure 1 (continued). Note the HeII 4686 nebular residual in NGC 5189 and the chip gaps at $\lambda = 4955 \text{ \AA}$ to 4961 \AA and $\lambda = 5142 \text{ \AA}$ to 5161 \AA .

Table 2. Table showing the log of observations for the sample.

Object	MJD (Days)	Date (MM/DD/YYYY)	Exp. time (s)	Grating	λ (Å)	Dispersion (Å pix ⁻¹)	$\langle S/N \rangle$	FWHM (Å)
Hen 2-113	56063.812846	05/16/2012	300	4	4260-5115	0.49	25	1.5
	56063.823819	05/16/2012	900	"	4257-5115	0.49	50	1.1
	56063.839880	05/16/2012	900	"	4257-5115	0.49	28	1.1
	56063.869755	05/16/2012	1200	"	4257-5115	0.49	48	1.3
	56064.122231	05/16/2012	1500	"	4257-5115	0.49	31	1.3
	56064.801191	05/17/2012	1500	"	4257-5115	0.49	34	1.3
	56069.996481	05/22/2012	1500	"	4257-5117	0.49	30	1.3
	56106.823001	06/28/2012	1500	6	4025-5936	1.10	40	2.8
	56108.917004	06/30/2012	1500	"	4055-5965	1.10	80	2.6
	56108.928125	06/30/2012	1500	"	4036-5950	1.10	83	2.7
	56109.813025	07/01/2012	1800	"	5722-7565	1.06	79	2.4
	56111.030991	07/02/2012	1500	"	5722-7567	1.06	53	2.5
Hen 2-99	56068.820887	05/21/2012	1800	6	4025-5937	1.10	43	2.7
	56106.744197	06/28/2012	1800	"	4036-5947	1.10	45	2.7
	56107.745127	06/29/2012	1800	"	4036-5950	1.10	25	2.7
	56108.866659	06/30/2012	2400	"	5722-7565	1.06	29	2.5
	56109.747499	07/01/2012	2400	"	5721-7565	1.06	23	2.5
	56110.976449	07/02/2012	2400	"	4034-5948	1.10	38	2.6
	56111.821737	07/03/2012	860	"	4033-5947	1.10	25	2.7
Hen 3-1333	56106.927875	06/28/2012	1200	6	4036-5947	1.10	61	2.6
	56108.109317	06/29/2012	1800	"	4032-5940	1.10	46	2.7
	56108.899327	06/30/2012	1800	"	5722-7567	1.06	34	2.4
	56109.131929	07/01/2012	2400	"	5722-7570	1.06	50	2.4
	56109.873401	07/01/2012	1500	"	5722-7572	1.06	50	2.4
	56109.996351	07/01/2012	1500	"	4035-5948	1.10	64	2.7
	56111.057141	07/03/2012	1500	"	4029-5948	1.10	89	2.6
NGC 5315	56068.848701	05/21/2012	1500	6	4025-5939	1.10	30	2.7
	56106.777051	06/28/2012	1500	"	4036-5947	1.10	24	2.7
	56109.782759	07/01/2012	2400	"	4033-5944	1.10	24	2.7
	56110.773799	07/02/2012	2400	"	4014-5929	1.10	23	2.7
PMR 2	56106.715497	06/28/2012	1800	"	4036-5948	1.10	32	2.6
	56107.709237	06/29/2012	1800	"	4036-5948	1.10	27	2.6
	56108.713127	06/30/2012	2400	"	5722-7565	1.06	40	2.5
	56109.713509	07/01/2012	2400	"	5722-7565	1.06	30	2.4
	56109.843839	07/01/2012	2400	"	5722-7565	1.06	15	2.6
	56110.721211	07/02/2012	1800	6	4036-5948	1.10	37	2.7
	56110.735899	07/02/2012	2400	"	4015-5927	1.10	36	2.7
NGC 5189	56672.581101	01/15/2014	900	PG2300	4440-5462	0.32	63	2.1
	56674.596367	01/17/2014	900	"	"	"	69	2.1
	56677.556460	01/20/2014	900	"	"	"	51	2.1
	56685.583323	01/28/2014	900	"	"	"	87	2.1
	56698.625846	02/10/2014	900	"	"	"	65	2.1
	56700.550927	02/12/2014	900	"	"	"	47	2.1
	56701.611668	02/13/2014	900	"	"	"	59	2.1
	56704.578300	02/16/2014	900	"	"	"	44	2.1
	56705.486876	02/16/2014	900	"	"	"	61	2.1
	56705.506708	02/17/2014	900	"	"	"	44	2.1
	56706.566535	02/18/2014	900	"	"	"	63	2.1
	56707.556766	02/19/2014	900	"	"	"	65	2.1
	56731.589104	03/15/2014	900	"	"	"	55	2.1
	56733.414920	03/16/2014	900	"	"	"	89	2.1

used for cross-correlation because nebular lines may dilute any shifts measurable from the stellar lines. Table 3 gives an outline of the wavelength ranges used for cross-correlation. Following the Foellmi et al. (2003) method we used the bisector method to determine the absolute zero-point velocity of T2 to put all the other measurements into heliocentric

velocities. Table 4 summarises the strongest stellar emission lines chosen for this purpose together with their mean heliocentric velocity and the mean RV of the nebula measured separately from our observations. The online tool VOSPEC (Osuna et al. 2005) was used for bisecting the chosen emission line in the template spectrum and to obtain the absolute

Table 3. The wavelength ranges chosen for the cross-correlations of stellar lines. The empty fields (“-”) mean either no observations were made in that particular wavelength range or not enough spectra were available for cross-correlation.

Object	Blue wavelength range (Å)	Red wavelength range (Å)
Hen 2–113	4477-4705 & 5050-5500	6064-6372 & 6736-7050
Hen 3–1333	4500-4720 & 4785-5420	6000-6288 & 6734-7057
Hen 2–99	4500-5740	6630-7300 & 6000-6490
NGC 5315	4477-4705 & 5050-5500	-
PMR 2	4477-5400	6321-6536 & 6838-7055
NGC 5189	5200-5450	-

RV of the template using the central wavelength (observed) and rest wavelength obtained from the NIST website⁴. The fraction of the emission line height (h) used to obtain the middle point varied for different objects. For different lines, an estimate was made to the portion which is more or less vertical i.e. $\sim 0.3h$ to $0.8h$. Seemingly, VOSPEC was introducing a ~ 0.5 Å shift in the template, but we corrected for this in our analysis and it does not affect our results.

3.2 Construction of RV time-series

The main outputs by XCSAO are the RV shift in km s^{-1} of the object spectrum relative to the T2 template together with the height of the cross-correlation peak and the associated error in km s^{-1} . In summary, the velocity obtained by the bisector represents the mean stellar velocity and the RVs are computed using:

$$v_i = v_{xcsao} + v_{bisector} + v_{hcv}$$

Where v_{xcsao} is the RV output by XCSAO, $v_{bisector}$ is the stellar mean RV calculated using the bisector method and v_{hcv} is the heliocentric velocity correction.

The error in the individual RVs (v_i) was computed in quadrature using the equation:

$$\Delta v_i = \sqrt{\Delta v_{xcsao}^2 + \Delta v_{bisector}^2}$$

Where $\Delta v_{bisector}$ is the error measurement for the bisector method and Δv_{xcsao} is the error output by XCSAO as described by Kurtz & Mink (1998). A peak is selected by fitting a smooth curve with accurate values of δ (the central value), h (the height of the central peak) and w (the FWHM of the peak). Kurtz & Mink (1998) assumed a sinusoidal noise profile, with the halfwidth of the sinusoid equal to the halfwidth of the correlation peak. The mean error output by XCSAO is a single velocity measurement and is given by:

$$error = \frac{3}{8} \frac{w}{(1+r)}$$

Where w is the FWHM of the correlation peak and r is defined in Tonry & Davis (1979), as the ratio of the height of the true peak to the average peak.

4 RESULTS

4.1 RV time series

Tables B1 and B2 list the resultant RV time-series for each object. Figures 3 and 4 display the data graphically. We emphasise that since the [WR] emission lines are formed in the wind, the absolute values of the velocities may not be meaningful (especially when compared against the nebular RVs). To quantify the variability level observed in each object, we conducted a χ^2 analysis of the RV time-series based on a null hypothesis which is discussed in detail by Trumpler & Weaver (1953). These authors recommend a standard χ^2 computation, from the reduced χ_{n-1}^2 (where n is the number of RV measurements and $n-1$ is the number of degrees of freedom) which leads to an estimate of the probability that the star’s RV is variable. In summary, let’s say the hypothesis to be tested is H : *The semi-amplitude “A” of a radial velocity variation equals zero.*, i.e. there is no statistical difference between the observed values (x_j) and the expected values (\bar{x}). Then alternatively, the hypothesis is that $A > 0$. The test for H is such that:

(i) P_I is the probability of *rejecting* H when H is true (i.e. saying $A > 0$, when $A = 0$). Now, if we set $\alpha = 0.05$ arbitrarily, then in this case, $P_I \leq \alpha$.

(ii) P_{II} is the probability of *accepting* H when H is false (i.e. saying $A = 0$, when $A > 0$). In this case P_{II} must be a minimum, no matter which orbit. So, maximizing β (where $\beta = 1 - P_{II}$, is the probability that the test will reject H when H is false) in the vicinity of $A = 0$.

The compromise consists of allowing the value of β to be at least as large as α . Hence, the criterion for rejection is: reject the hypothesis that $A = 0$ whenever:

$$\sum_{j=1}^n \frac{(x_j - \bar{x})^2}{\sigma_i^2} \geq \chi_{\alpha, n-1}^2$$

where

- $\chi_{\alpha, n-1}^2$ is the standard χ^2 value for $n - 1$ degrees of freedom and probability, $P = \alpha$.
- \bar{x} is the stellar mean (Expected value).
- x_j is the individual values for the stellar RVs.
- σ_i the individual errors in the RVs.

The null hypothesis simply states that there is no statistical difference between the observed value (data) and the expected value which in our case is the stellar mean. The main point is to either accept or reject the null hypothesis with a given probability based on a critical value ($\alpha = 0.05$). If the value of the observed χ^2 is less than $\chi_{0.05, n-1}^2$, we will accept the null hypothesis with a probability of 95%. This means that we are 95% sure that the variations in the RV are random. Contrarily, if the observed χ^2 is greater than $\chi_{0.05, n-1}^2$ then we will reject the null hypothesis with a probability of 95%, meaning the RV is highly variable. The convention we will use here is looking at the probability of accepting the null hypothesis.

The above variability test was run on the 6 objects, assuming the stellar mean is the expected mean and the results are shown in Table 5. For each of them, the χ_{obs}^2 (observed Chi-squared) was computed and the probability that the object is variable $P(\chi_{obs}^2 \geq \chi_{n-1}^2)$ was obtained. For some stars,

⁴ <http://www.nist.gov/pml/data/asd.cfm>

Table 4. The weighted mean radial velocities for stellar and nebular emission features of each object. The nebular lines used are H α , H β , H δ , H γ , NII-6583 and OIII-4959.

Object	Stellar	λ_{rest} (Å)	$\langle RV_{stellar} \rangle$ (km s ⁻¹)	Nebular	$\langle RV_{neb} \rangle$ (km s ⁻¹)
Hen 2-113	CII	4267.26	-60±4	H α , H β , H δ , H γ , NII	-63±2
Hen 3-1333	CIII	5695.19	-43±4	H α , H β , H γ , NII	-66±10
Hen 2-99	CIII	5695.19	-56±12	H α , H β , NII	-95±13
NGC 5315	HeI	4471.47	84±15	H α , H β , H γ , NII, OIII	-24±8
PMR 2	CII	4267.18	4±5	H α , H β , NII	-66±23
NGC 5189	OVI	5290.65	23±40	H β	-8±4

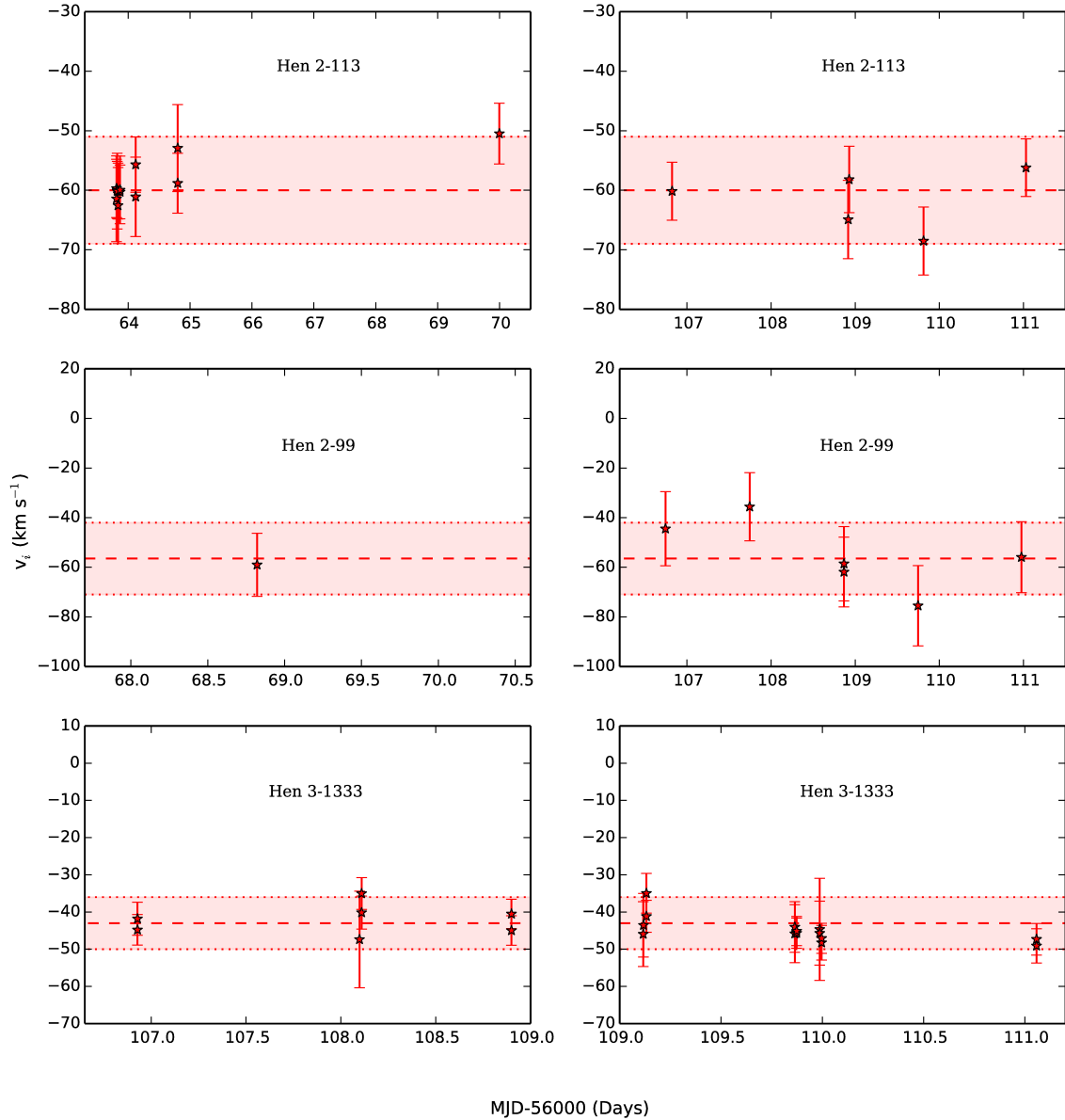


Figure 3. Measured RV time-series for the nuclei of Hen 2-113, Hen 2-99 and Hen 3-1333.

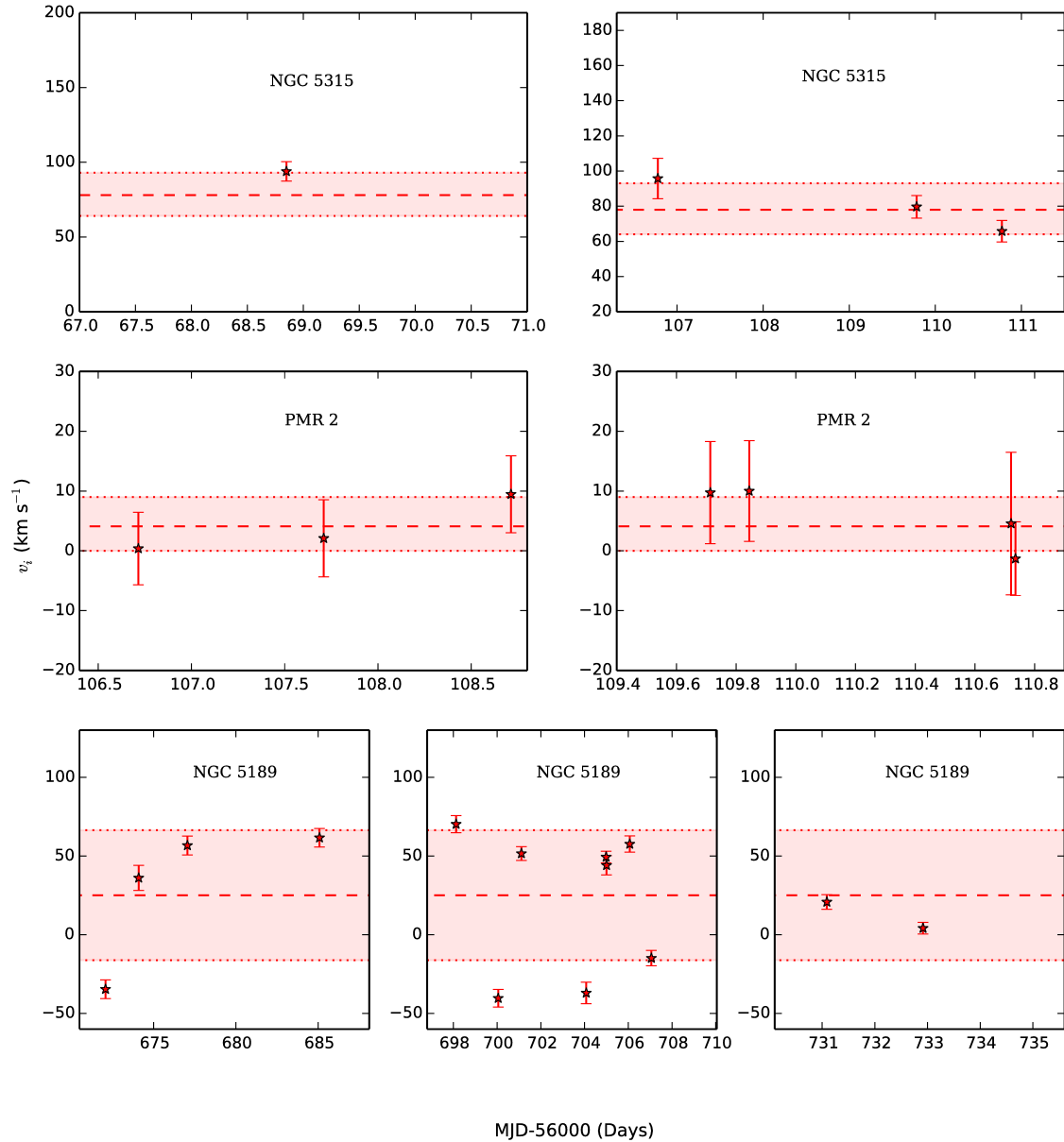


Figure 4. Measured RV time-series for the nuclei of NGC 5315, PMR 2 and NGC 5189.

the RV variability was so large that it becomes obvious with only a few observations to decide whether it is a binary or not. However, in most cases we lack sufficient observations to properly constrain the amount of variability in the RV. In cases where small random fluctuations in the RV from the mean occur, which we would expect due to instrumental uncertainties or wind variability, we would identify the RV as being constant. However, a highly variable RV from the mean would be one having large enough RV variations that cannot be assigned solely to random variations. In the case

of a close binary CSPN we require a statistically significant periodic signature in the RV time-series to be present.

The objects observed with the SAAO 1.9-m are not sufficiently variable to prove a binary companion is present at this time, however two objects stand out from the rest. Hen 2-99 has stellar RV shifts with a peak-to-peak value of the order 30 km s⁻¹ from the mean and a hint of periodicity is seen with a peak-to-peak of ~ 53 km s⁻¹. A sinusoid fits reasonably well with the RV of Hen 2-99 with a period of 5.3 d. More data is needed to confirm this period. Similarly, NGC 5315 shows much higher RV variability ($P_{\text{null}} = 1\%$),

Table 5. Results of the variability test carried on individual objects. Column 1 shows the object name, the 2nd column is the number of RV measurements (degrees of freedom+1), the 3rd column is the mean RV, the 4th column is the standard deviation in the RV, the 5th column is the observed χ^2 and column 6 shows the probability of accepting the null hypothesis based on the χ^2 value.

Object	n	$\langle \text{RV} \rangle$ (km s ⁻¹)	σ (km s ⁻¹)	χ^2_{obs}	P_{null}
Hen2-113	18	-59.5	4.1	8.8	94%
Hen3-1333	15	-44.1	4.4	0.2	100%
Hen2-99	8	-55.7	12.0	4.5	72%
NGC 5315	4	87.3	14.0	15.3	1%
PMR 2	7	4.0	4.8	3.0	80%
NGC 5189	14	23.2	40.1	690	0%

but we have only 4 epochs for this object. The non-periodic and relatively small amplitude RV shifts in the remaining objects that we see are most probably due to stochastic wind variability (e.g. Grosdidier et al. 2000, 2001).

NGC 5189 is the only object in the sample that shows very high RV variability with a peak-to-peak velocity of the order of 120 km s⁻¹ (see Fig. 4). From the χ^2 variability analysis in Table 5 and Fig. 4 it is quite clear that it is the only object which shows 100% variability. The following section further analyses this unique dataset.

5 THE CLOSE BINARY CS OF NGC 5189

5.1 Orbital period analysis and mass function

Since our data is not evenly sampled, we used the Lomb-Scargle (Lomb 1976; Scargle 1982) method to search for an orbital period. The Lomb-Scargle method is mainly based on a least-squares fit of sinusoids (Press & Rybicki 1989). Figure 5 shows four significant peaks in the periodogram at periods 4.04 days, 3.54 days, 1.32 days and 0.80 days. However, we find that the 3.54 day, 1.32 day and 0.80 day peaks are most likely to be aliases, as they do not persist when we ran the Lomb-Scargle for a second time after extracting the 4.04 day period. Moreover, to test the validity of the periods, we further analysed the data according to the method described by Tanner (1948). Assuming the actual period is 4.04 d, both the 1.32 d and the 0.8 d periods satisfy Equation 2 in Tanner (1948). Based on the relatively high value χ^2 of 8.3 for the 3.54 day period sinusoid fit, we further reject this period. This leaves us with the best period being 4.04 d which has the lowest χ^2 of 3.0 out of all periods.

A significance test was also carried out on the periods found using a Monte-Carlo simulation, where a random number generator was used to scramble the original radial velocities within one standard deviation, creating 10000 randomised RV curves of the same structure. A Lomb-Scargle analysis was then performed on the randomised RV curves and the highest powers were recorded for each of them. The powers were then sorted in ascending order after which the 90%, 99% and 99.9% significance levels were obtained (displayed as horizontal lines in Fig. 5). The only period which was found to be above the 99.9% level and acceptable as per the sinusoid model fit was the 4.04 day.

The second panel in Figure 5 is a sinusoid model determined from fitting the data folded on the 4.04 day period in phase space. We used the MPFIT and MPFITFUN IDL codes designed to perform a Levenberg-Marquardt least-squares fit of a user supplied model to a function (Markwardt 2012). The main fitting was done by MPFIT after specifying a set of initial parameters. Given the data and their uncertainties, MPFITFUN computes the best set of model parameters which match the data and returns them in an array. In time space we determined a 4.04 day period fit of the form $A \sin(2\pi f - \phi) + B$ to the data where A denotes the amplitude, f is the frequency fixed at 0.247 day⁻¹, ϕ is the phase and B is the mean, with $A = 62.3$ km s⁻¹, $\phi = 0.43$ and $B = 14.0$ km s⁻¹. This corresponds to an ephemeris determined from the minimum radial velocity at MJD (min RV) = $(2456700.24 \pm 0.02) + (4.04 \pm 0.1)E$. The error in the orbital period was determined by fitting a gaussian with a mean of 4.04 d and a standard deviation of 0.1 d to the peak period in the periodogram. The bottom two panels of Fig. 5 shows this fit along with the RV time-series data showing the reasonable agreement to our observations. Figure 6 gives another graphical representation of the periodic motion in the RV time-series data of NGC 5189. The trail diagrams are plotted over 2 phases using the motion of the OVI-5290 stellar emission line and, for comparison, the static H β nebular emission line.

In the case of close-binaries with a good sinusoidal fit, it is fair to assume a low ($e \ll 1$) or zero eccentricity. In this case the mass function of two stars of masses m_1 and m_2 , where only one of the stars is visible in the spectrum (single-line spectroscopic binaries) is described by:

$$f(m_1, m_2) = \frac{m_2^3}{(m_1 + m_2)^2} \sin^3 i = \frac{P}{2\pi G} v_1^3$$

where P is the orbital period (4.04 ± 0.1 d), i is the inclination of the orbital plane to the line of sight, and v_1 is the semi-amplitude of the RV curve ($v_1 = 62.3 \pm 1.3$ km s⁻¹).

Table 6 lists companion masses m_2 calculated for a range of inclination values and an adopted m_1 mass of 0.596 M_\odot for the [WO1] primary. The value of m_1 was calculated as an average of the masses of Miller Bertolami & Althaus (2006) evolutionary tracks either side of the location of NGC 5189 in figure 13 of Keller et al. (2014). There are several caveats associated with this assumption. Firstly, the mass estimates derived from interpolating between evolutionary tracks are distance dependent and distances to PNe are notoriously uncertain. Keller et al. (2014) adopted a distance of 0.55 kpc to NGC 5189 (Stanghellini et al. 2008), but the distance may be as large as 1.44 ± 0.27 kpc based on extinction and kinematic distance estimates (Frew 2008). The luminosity would therefore increase from $\sim 2.73 L_\odot$ (Keller et al. 2014) to $\sim 3.86 L_\odot$ (Frew 2008), resulting in a mass closer to $\sim 0.62 M_\odot$. However, it is not necessarily a matter of adopting this mass as this method of estimating CSPNe masses does not agree well with spectroscopic mass estimates for CSPNe (see section 4.2.3 of Moe & De Marco 2006 and ref. therein), underlying the intrinsic unreliability of such model-dependent methods. Finally, the evolutionary tracks assume single star evolution which may not apply to a post-CE binary such as the nucleus of NGC 5189.

In summary, these caveats make it difficult to choose any ‘best’ value for m_1 . As the orbital inclination of the neb-

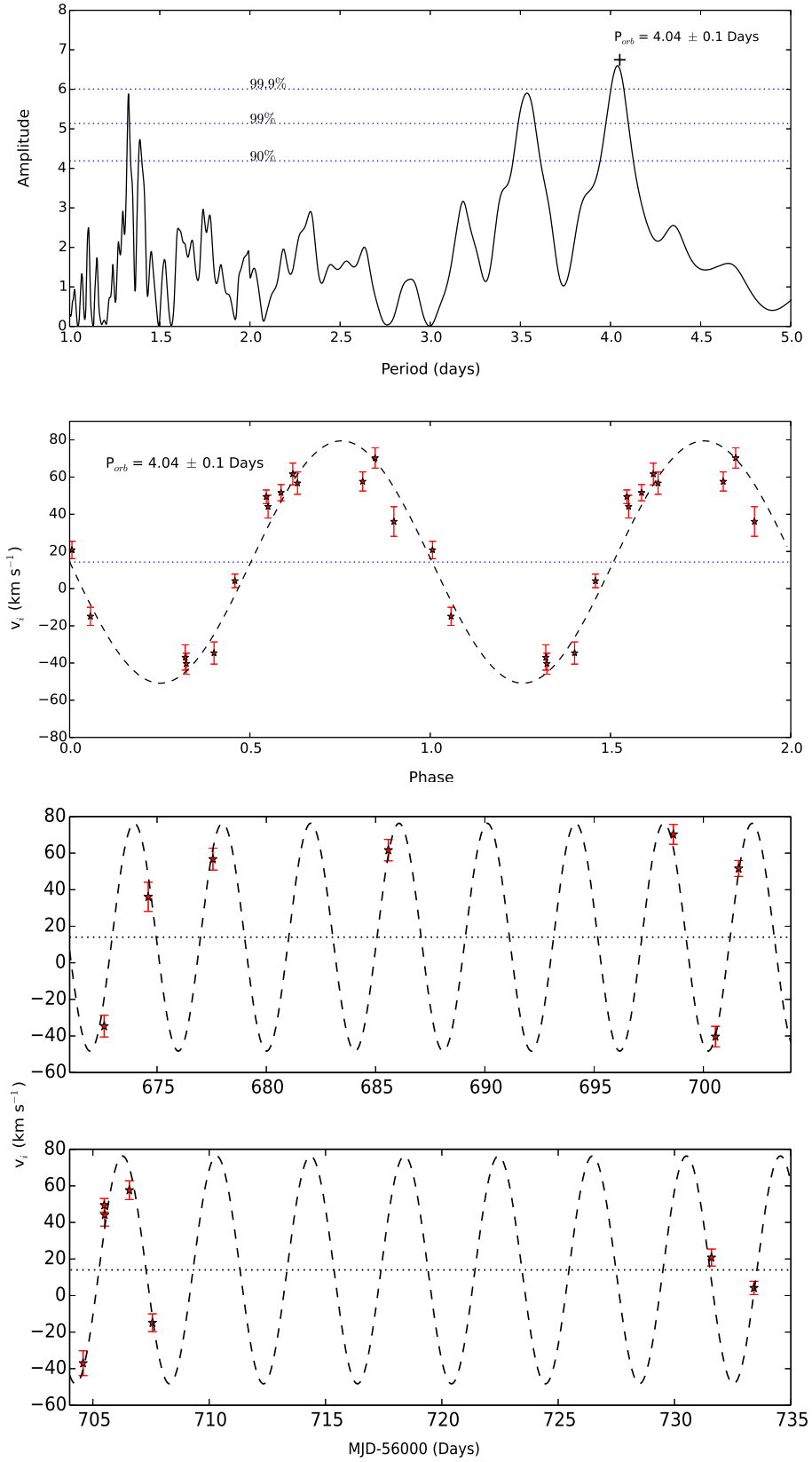


Figure 5. **Top:** The Lomb-Scargle periodogram showing the significance levels of 90%, 99% and 99.9%. **Middle:** The radial velocity folded on the 4.04 day period fitted with a sinusoidal model. **Bottom:** Plot of the radial velocities folded on the 4.04 day period fitted with a sinusoid.

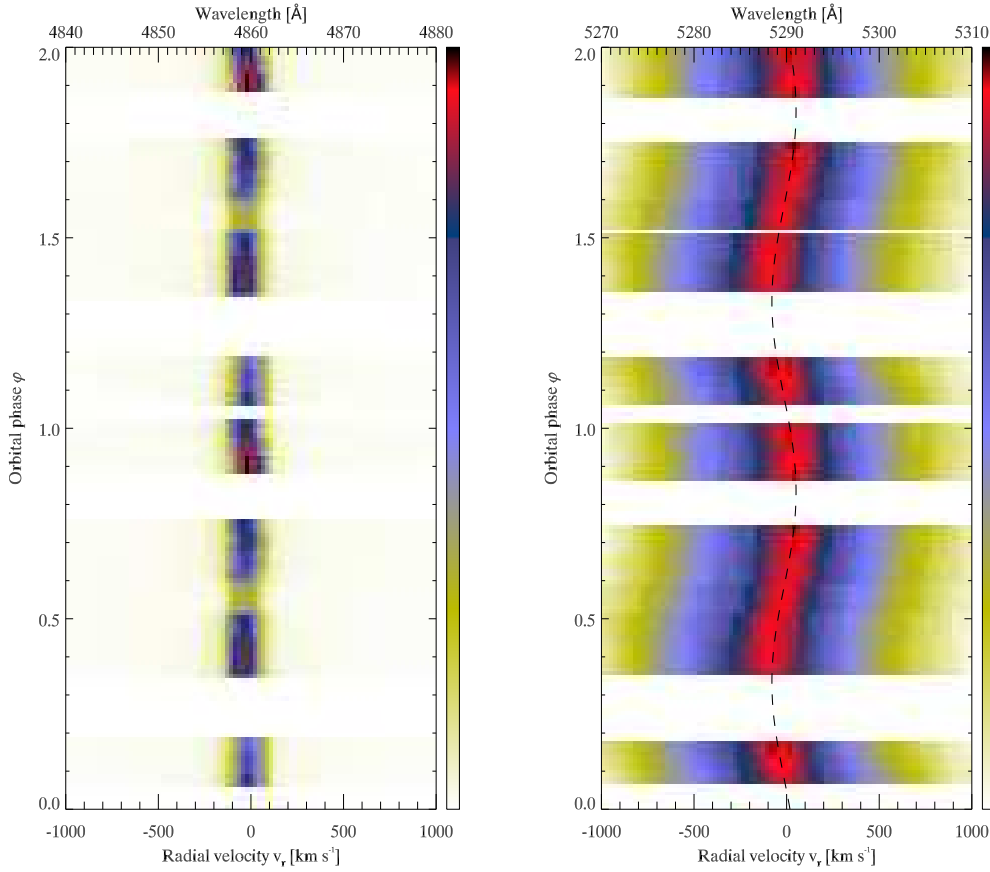


Figure 6. Left: Trail diagram of the nebular H β line. Right: Trail diagram of the stellar OVI-5290 emission line. The dashed line shows the sinusoidal fit to the RV curve in phase space.

ula is currently unconstrained (Sabin et al. 2012), it is only possible in this work to give an indication of plausible companion masses. The unknown inclination introduces a much larger uncertainty in m_2 than the small uncertainty in m_1 . Therefore, for the purposes of this work, it is reasonable to retain the adopted value of $m_1 = 0.596 M_\odot$ that is essentially the same as the standard mass assumed for CSPNe of $0.6 M_\odot$ (e.g. Crowther et al. 2006; Crowther 2008). Even if a slightly more massive m_1 were adopted, it would only result in a small increase in m_2 .

5.2 Nature of the companion

We give a summary of the properties of the CS of NGC 5189 in Table 7 and Table 8 gives the orbital parameters derived in this work. The mass function puts a lower limit on m_2 ($0.5 M_\odot \pm 0.01$) which is reached only if the system is edge-on with $i = 90^\circ$. For inclinations less than 40 degrees we find improbably high values of m_2 , suggesting these inclinations can be discarded. At other inclinations the possible companions are a main sequence star or a WD. It may be possible for an orbital period of 4.04 d that a main sequence companion could produce an irradiation effect, especially given the 165 kK temperature of the [WO1] component. This effect

Table 6. Companion masses (m_2) for NGC 5189 for a variety of orbital inclination angles.

Inclination ($^\circ$)	m_2 (M_\odot)	Δm_2 (M_\odot)
30	1.56	0.03
35	1.21	0.02
40	0.99	0.02
45	0.84	0.01
50	0.74	0.01
55	0.67	0.01
60	0.61	0.01
65	0.57	0.01
70	0.54	0.01
75	0.52	0.01
80	0.51	0.01
85	0.50	0.01
90	0.50	0.01

could be up to 0.1-0.2 mag (De Marco et al. 2008), but this has not yet been observed (e.g. Ciardullo & Bond 1996). There is also no evidence to suggest a cool companion is present since the intrinsic ($V - I$) colour of -0.32 ± 0.08 is typical of hot blue CSPNe ($(V - I)_0 \sim -0.4$, Ciardullo

Table 7. Properties of NGC 5189 and the [WO1] primary.

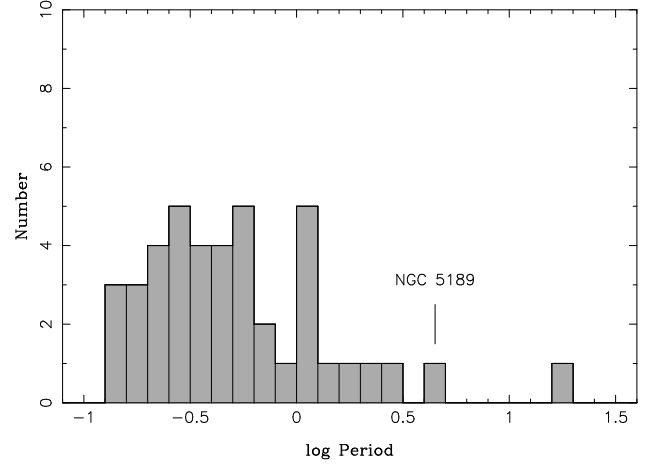
PN G	307.2–03.4	
$c(H\beta)$	0.47 ± 0.08	Garcia-Rojas et al. (2012)
V (mag)	14.53	Ciardullo et al. (1999)
I (mag)	14.35	Ciardullo et al. (1999)
$(V - I)_0$	-0.32 ± 0.08	This work
Type	[WO1]	Crowther et al. (1998)
v_∞ (km s $^{-1}$)	2500 ± 250	Keller et al. (2014)
T_{eff} (kK)	165^{+18}_{-8}	Keller et al. (2014)
m_1 (M_\odot)	0.596	Keller et al. (2014)

Table 8. Orbital parameters of NGC 5189.

$P_{\text{orb}}(d)$	4.04 ± 0.1
e	0 (fixed)
K (km s $^{-1}$)	62.3 ± 1.3
γ (km s $^{-1}$)	14 ± 1
m_2 (M_\odot)	≥ 0.5
T_0 (MJD)	56699.74 ± 0.02

et al. 1999). The intrinsic faintness of the primary, namely $M_V = +2.7$ to $+4.8$ mag for $d = 1.44$ kpc (Frew 2008) or 0.55 kpc (Stanghellini et al. 2008), respectively, also means that it is unlikely that a cool companion is hiding in the glare of the primary. Although the orbital inclination is currently unconstrained (Sabin et al. 2012), we can estimate an intermediate inclination of 45 degrees based on the apparent nebular morphology, i.e. the relatively symmetrical inner nebula with a pinched waist (see Sect. 5.3) and that the collimated outflows are neither completely inside or outside the nebula. The companion is therefore likely to be a slightly more massive WD of $\sim 0.9 M_\odot$, comparable to the companion discovered in Fleming 1 (Boffin et al. 2012).

The 4.04 d orbital period of NGC 5189 is one of the longest currently known amongst post-CE CSPNe (Fig. 7) and falls into the zone with periods $\gtrsim 1$ day where there is a substantial deficit of post-CE binaries compared to CE population synthesis models (Rebassa-Mansergas et al. 2008; Miszalski et al. 2009a; Davis et al. 2010; Nebot Gómez-Morán et al. 2011). There are two possible interpretations for the position of NGC 5189 in the post-CE orbital period distribution. One is that the longer period is a one-off coincidence as in NGC 2346 and this would be in line with the observed deficit. The other possibility is that NGC 5189 reflects the tip of an iceberg where most [WR] close binaries would have similarly long orbital periods (or longer). This could be explained by the stronger and more extended wind of the [WR] component that could interact with the companion (e.g. via wind Roche-lobe overflow, Mohamed & Podsiadlowski 2007, 2011). If the interaction were to facilitate the CE phase at greater orbital separations than in the average post-CE CSPN (WD and main sequence), then the resultant orbital period might be longer than the average. At present with only two [WR] post-CE CSPNe known, it is difficult to decide which of these two possibilities is correct.

**Figure 7.** Orbital period distribution of published close binary CSPNe (see Appendix A1).

5.3 The post-CE nebular morphology

The main reason for including NGC 5189 in our study was that it contains all the hallmarks of post-CE nebulae as first outlined by Miszalski et al. (2009b). These hallmarks include low-ionisation structures (LIS; see e.g. Gonçalves et al. 2001), collimated outflows or jets and bipolar nebulae (see also Miszalski et al. 2011b and Miszalski 2012). Additional recent discoveries of post-CE nuclei in other PNe have further reinforced these hallmarks (Corradi et al. 2011; Miszalski et al. 2011a,b,c; Boffin et al. 2012; Jones et al. 2014). The abundance of LIS filaments in NGC 5189 (e.g. Sabin et al. 2012), the majority of which point to the central star, is exactly what we see in NGC 6326 (Miszalski et al. 2011b) and similarly high levels of LIS are also seen in NGC 6778 (Miszalski et al. 2011b; Guerrero & Miranda 2012) and Hen 2-11 (Jones et al. 2014). Secondly, Sabin et al. (2012) demonstrated that the outermost LIS of NGC 5189 have the most extreme velocities of the nebula. Combined with the central S-shaped feature, these outermost LIS are symptomatic of a precessing outflow (e.g. Lopez et al. 1993) that is best explained by jets being launched from a precessing accretion disk around a companion (Cliffe et al. 1995; Raga et al. 2009; Boffin et al. 2012). Furthermore, leaving the LIS aside, the intrinsic morphology of NGC 5189 appears to be a bipolar outflow best seen in the [O III] emission line. It is pinched at the waist at the edges of the minor axis that is closely aligned with slit position 4 in figure 2 of Sabin et al. (2012). As emphasised in Miszalski et al. (2011b) with NGC 6326, there is a stark disconnect between the intrinsic morphology of the nebula and the LIS, the latter of which may form separately to the diffuse components.

6 CONCLUSIONS

We carried out an RV monitoring program of 6 Galactic [WR] CSPNe using a well established cross-correlation method successfully used in massive WR star studies (Foellmi et al. 2003). Four of the CSPNe in our sample are late-types ([WCL]) namely Hen 2-99, Hen 2-113, Hen 3-1333 and PMR 2, and two are early-type ([WCE]), namely the

CSPNe of NGC 5189 and NGC 5315. Our main conclusions are as follows:

(i) No significant variability was detected in Hen 2-113, Hen 3-1333 and PMR 2. Hen 2-99 may be variable with a putative periodicity of 5.3 d, but more observations are needed to further investigate. Similarly, NGC 5315 shows a much greater level of variability but will again require more observations to search for an orbital period.

(ii) NGC 5189 showed significant RV variability in stark contrast to the other objects in our sample. A significant period of 4.04 d was found from the Lomb-Scargle periodogram and fitting the phased data gave a peak-to-peak amplitude of $\sim 124 \text{ km s}^{-1}$. The orbital motion is clearly seen in the trailed diagram of the stellar O VI 5290 emission line compared against the static H β nebular emission line. The mass of the companion m_2 has a lower limit of $0.5 M_\odot$ and may be $\sim 0.9 M_\odot$ for a reasonable assumption of the nebular inclination of $i = 45$ degrees. A more massive WD companion is likely to be present, explaining the lack of an irradiation effect in previous photometric observations of the object. Further spatio-kinematic modelling of NGC 5189 as in Sabin et al. (2012) is strongly encouraged to further constrain the inclination and therefore companion mass.

(iii) The spectacular nebula of NGC 5189 further fits the trend for post-CE nebulae to be dominated by low-ionisation structures (e.g. NGC 6326, Miszalski et al. 2011) and to possess precessing outflows (e.g. Fleming 1, Boffin et al. 2012) as first outlined by Miszalski et al. (2009b). Several of the PNe with [WR] nuclei discussed in Miszalski et al. (2009b) are therefore excellent candidates for RV monitoring to discover new [WR] binaries.

(iv) The discovery of a second close binary system containing a [WR] component strongly suggests mergers are not involved in the formation of most [WC] CSPNe. It remains to be seen whether [WN] CSPNe are binary systems. Indeed, the relatively long orbital period of NGC 5189 could be either a one-off coincidence (e.g. NGC 2346) or alternatively it could indicate that potentially many more [WR] binaries may be found if appropriate RV monitoring surveys are conducted. We speculate that wind interactions between the [WR] component and its companion (e.g. wind Roche-lobe overflow) may be responsible for the longer period. Further RV monitoring of [WR] CSPNe is urged to try and discover more systems to place constraints on the formation of [WR] CSPNe.

7 ACKNOWLEDGEMENTS

We would like to thank Enrico Kotze for producing the trailed diagrams included in this paper. We acknowledge the very helpful discussions and support of Itumeleng Mongageng, Rudi Kuhn, Lee Townsend, Paul Crowther, Orsola De Marco and Noam Soker. We thank Prof. R. H. Méndez for his constructive referee report that has helped improve this paper. We are grateful to the SAAO IT team for their wonderful support in terms of computer hardware for the paper write-up. RM thanks the University of Cape Town for financial support to write this paper funded by the paper grant: Postgraduate Publication Incentive (PPI) funding. RM is grateful to the Square Kilometre Array (SKA) and National Research Foundation (NRF) for their financial

support of the MSc thesis this work is based on. VM acknowledges financial support from the NRF, South Africa. The observations reported in this paper were obtained with the SAAO 1.9-m telescope and the Southern African Large Telescope (SALT).

REFERENCES

- Acker, A., & Neiner, C. 2003, *A&A*, 403, 659
- Balick, B., & Frank, A. 2002, *ARA&A*, 40, 439
- Balick, B. 2007, *Asymmetrical Planetary Nebulae IV*, <http://www.astro.washington.edu/users/balick/PNIC/>
- Blöcker, T. 2001, *Ap&SS*, 275
- Boffin, H. M. J., Miszalski, B., Rauch, T., et al. 2012, *Science*, 338, 773
- Bond, H. E., Liller, W., & Mannery, E. J. 1978, *ApJ*, 223, 252
- Bond, H. E. 1985, *Cataclysmic Variables and Low-Mass X-ray Binaries*, 113, 15
- Bond, H. E., & Grauer, A. D. 1987, *IAU Colloq. 95: Second Conference on Faint Blue Stars*, 221
- Bond, H. E., & Livio, M. 1990, *ApJ*, 355, 568
- Bond, H. E. 2000, *Asymmetrical Planetary Nebulae II: From Origins to Microstructures*, 199, 115
- Buckley, D. A. H., Swart, G. P., & Meiring, J. G. 2006, *SPIE*, 6267, 32
- Burgh, E. B., Nordsieck, K. H., Kobulnicky, H. A., et al. 2003, *SPIE*, 4841, 1463
- Chesneau, O., Collioud, A., De Marco, O., et al. 2006, *A&A*, 455, 1009
- Ciardullo, R., & Bond, H. E. 1996, *AJ*, 111, 2332
- Ciardullo, R., Bond, H. E., Sipior, M. S., et al. 1999, *AJ*, 118, 488
- Cliffe, J. A., Frank, A., Livio, M., & Jones, T. W. 1995, *ApJL*, 447, L49
- Corradi, R. L. M., Sabin, L., Miszalski, B., et al. 2011, *MNRAS*, 410, 1349
- Corradi, R. L. M., Rodríguez-Gil, P., Jones, D., et al. 2014, *MNRAS*, 441, 2799
- Cozens, G., Walsh, A., & Orchiston, W. 2010, *Journal of Astronomical History and Heritage*, 13, 59
- Crawford, S. M., Still, M., Schellart, P., et al. 2010, *Proc. SPIE*, 7737E, 54
- Crowther, P. A., De Marco, O., & Barlow, M. J. 1998, *MNRAS*, 296, 367
- Crowther, P. A., Morris, P. W., & Smith, J. D. 2006, *ApJ*, 636, 1033
- Crowther, P. A. 2008, *Hydrogen-Deficient Stars*, 391, 83
- Davis, P. J., Kolb, U., & Willems, B. 2010, *MNRAS*, 403, 179
- De Marco, O., & Soker, N. 2002, *PASP*, 114, 602
- De Marco, O., Barlow, M. J., & Cohen, M. 2002, *ApJ*, 574, L83
- De Marco, O., Bond, H. E., Harmer, D., & Fleming, A. J. 2004, *ApJ*, 602, L93
- De Marco, O. 2008, *Hydrogen-Deficient Stars*, 391, 209
- De Marco, O., Hillwig, T. C., & Smith, A. J. 2008, *AJ*, 136, 323
- De Marco, O. 2009, *PASP*, 121, 316
- Drake, A. J., Gänsicke, B. T., Djorgovski, S. G., et al. 2014, *MNRAS*, 441, 1186
- Drilling, J. S. 1985, *ApJL*, 294, L107
- Evans, D. S. 1968, *Monthly Notes of the Astronomical Society of South Africa*, 27, 37
- Foellmi, C., Moffat, A. F. J., & Guerrero, M. A. 2003, *MNRAS*, 338, 360
- Frew, D. J. 2008, Ph.D. Thesis, Macquarie University
- Frew, D. J., Bojčić, I. S., Parker, Q. A., et al. 2014, *MNRAS*, 440, 1345
- García-Rojas, J., Peña, M., Morisset, C., Mesa-Delgado, A., & Ruiz, M. T. 2012, *A&A*, 538, A54
- Gonçalves, D. R., Corradi, R. L. M., & Mampaso, A. 2001, *ApJ*, 547, 302
- González Pérez, J. M., Solheim, J.-E., & Kamben, R. 2006, *A&A*, 454, 527
- Górny, S. K. 2014, *A&A*, in press, arXiv:1406.1048
- Grauer, A. D., & Bond, H. E. 1983, *ApJ*, 271, 259
- Grauer, A. D., Bond, H. E., Ciardullo, R., & Fleming, T. A. 1987, *BAAS*, 19, 643
- Grosdidier, Y., Acker, A., & Moffat, A. F. J. 2000, *A&A*, 364, 597
- Grosdidier, Y., Moffat, A. F. J., Blais-Ouellette, S., Joncas, G., & Acker, A. 2001a, *ApJ*, 562, 753
- Guerrero, M. A., & Miranda, L. F. 2012, *A&A*, 539, A47
- Hajduk, M., Zijlstra, A. A., & Gesicki, K. 2010, *MNRAS*, 406, 626
- Handler, G. 2003, *Interplay of Periodic, Cyclic and Stochastic Variability in Selected Areas of the H-R Diagram*, 292, 183
- Henize, K. G. 1967, *ApJS*, 14, 125
- Herwig, F. 2001, *Ap&SS*, 275, 15
- Hillwig, T. C., Bond, H. E., Afşar, M., & De Marco, O. 2010, *AJ*, 140, 319
- Hua, C. T., Dopita, M. A., & Martinis, J. 1998, *A&A S*, 133, 361
- Iben, I., Jr., & Livio, M. 1993, *PASP*, 105, 1373
- Ivanova, N., Justham, S., Chen, X., et al. 2013, *A&ARv*, 21, 59
- Jones, D., Boffin, H. M. J., Miszalski, B., et al. 2014, *A&A*, 562, A89
- Keller, G. R., Bianchi, L., & Maciel, W. J. 2014, *MNRAS*, 442, 1379
- Kniazhev, A. Y., Zijlstra, A. A., Grebel, E. K., et al. 2008, *MNRAS*, 388, 1667
- Kobulnicky, H. A., Nordsieck, K. H., Burgh, E. B., et al. 2003, *SPIE*, 4841, 1634
- Koesterke, L. 2001, *Ap&SS*, 275, 41
- Kurtz, M. J., & Mink, D. J. 1998, *PASP*, 110, 934
- Lagadec, E., Chesneau, O., Matsuura, M., et al. 2006, *A&A*, 448, 203
- Lawlor, T. M., & MacDonald, J. 2002, *Exotic Stars as Challenges to Evolution*, 279, 193
- Liebert, J., Tweedy, R. W., Napiwotzki, R., & Fulbright, M. S. 1995, *ApJ*, 441, 424
- Lomb, N. R. 1976, *Ap&SS*, 39, 447
- Lopez, J. A., Roth, M., & Tapia, M. 1993, *RMxAA*, 26, 110
- Lutz, J., Fraser, O., McKeever, J., & Tugaga, D. 2010, *PASP*, 122, 524
- Markwardt, C. 2012, *Astrophysics Source Code Library*, 8019
- Mendez, R. H., & Niemela, V. S. 1981, *ApJ*, 250, 240
- Mendez, R. H., Kudritzki, R. P., Herrero, A., Husfeld, D., & Groth, H. G. 1988, *A&A*, 190, 113
- Mendez, R. H., Herrero, A., & Manchado, A. 1990, *A&A*, 229, 152
- Méndez, R. H. 1991, *Evolution of Stars: the Photospheric Abundance Connection*, 145, 375
- Miller Bertolami, M. M., & Althaus, L. G. 2006, *A&A*, 454, 845

- Miller Bertolami, M. M., Althaus, L. G., Olano, C., & Jiménez, N. 2011, *MNRAS*, 415, 1396
- Miszalski, B. 2009, PhD Thesis, Macquarie University and Université de Strasbourg
- Miszalski, B., Acker, A., Moffat, A. F. J., Parker, Q. A., & Udalski, A. 2009a, *A&A*, 496, 813
- Miszalski, B., Acker, A., Parker, Q. A., & Moffat, A. F. J. 2009b, *A&A*, 505, 249
- Miszalski, B., Corradi, R. L. M., Boffin, H. M. J., et al. 2011a, *MNRAS*, 413, 1264
- Miszalski, B., Jones, D., Rodríguez-Gil, P., et al. 2011b, *A&A*, 531, A158
- Miszalski, B., R. L. M. Corradi, D. Jones, M. Santander-García, P. Rodríguez-Gil, M. M. Rubio-Díez 2011c, *Asymmetric Planetary Nebulae V*, arXiv:1009.2890
- Miszalski, B., Crowther, P. A., De Marco, O., et al. 2012, *MNRAS*, 423, 934
- Moe, M., & De Marco, O. 2006, *ApJ*, 650, 916
- Mohamed, S., & Podsiadlowski, P. 2007, 15th European Workshop on White Dwarfs, 372, 397
- Mohamed, S., & Podsiadlowski, P. 2011, *Why Galaxies Care about AGB Stars II: Shining Examples and Common Inhabitants*, 445, 355
- Morgan, D. H., Parker, Q. A., & Russeil, D. 2001, *MNRAS*, 322, 877
- Nagel, T., Schuh, S., Kusterer, D.-J., et al. 2006, *A&A*, 448, L25
- Napiwotzki, R., & Schoenberner, D. 1995, *A&A*, 301, 545
- National Institute of Standard and Technology (NIST), <http://www.nist.gov/pml/data/asd.cfm>, [Online; accessed in 2013]
- Nebot Gómez-Morán, A., Gänsicke, B. T., Schreiber, M. R., et al. 2011, *A&A*, 536, A43
- O'Donoghue, D., Buckley, D. A. H., Balona, L. A., et al. 2006, *MNRAS*, 372, 151
- Osuna, P., Barbarisi, I., Salgado, J., & Arviset, C. 2005, *Astronomical Data Analysis Software and Systems XIV*, 347, 198
- Phillips, J. P. 1984, *A&A*, 137, 92
- Phillips, J. P., & Reay, N. K. 1983, *A&A*, 117, 33
- Press, W. H., & Rybicki, G. B. 1989, *ApJ*, 338, 277
- Raga, A. C., Esquivel, A., Velázquez, P. F., et al. 2009, *ApJL*, 707, L6
- Rauch, T., Köppen, J., & Werner, K. 1994, *A&A*, 286, 543
- Rauch, T., Köppen, J., & Werner, K. 1996, *A&A*, 310, 613
- Rauch, T., Dreizler, S., & Wolff, B. 1998, *A&A*, 338, 651
- Rauch, T., Reiff, E., Werner, K., & Kruk, J. W. 2008, *Hydrogen-Deficient Stars*, 391, 135
- Rebassa-Mansergas, A., Gänsicke, B. T., Schreiber, M. R., et al. 2008, *MNRAS*, 390, 1635
- Reindl, N., Rauch, T., Werner, K., & Kruk, J. W. 2013, 18th European White Dwarf Workshop., 469, 143
- Reindl, N., Rauch, T., Werner, K., Kruk, J. W., & Todt, H. 2014, *A&A*, 566, A116
- Sabin, L., Vázquez, R., López, J. A., García-Díaz, M. T., & Ramos-Larios, G. 2012, *RMxAA*, 48, 165
- Sana, H., van Boeckel, T., Tramper, F., et al. 2013, *MNRAS*, 432, L26
- Santander-García, M., Rodríguez-Gil, P., Corradi, R.L.M., Jones, D., Miszalski, B., Boffin, H.M.J., Rubio-Díez, M.M., & Kotze, M.M., 2015, *Nature*, in press
- Scargle, J. D. 1982, *ApJ*, 263, 835
- Schoenberner, D. 1979, *A&A*, 79, 108
- Schnurr, O. 2008, Ph.D. Thesis,
- Schnurr, O., Moffat, A. F. J., Villar-Sbaiffi, A., St-Louis, N., & Morrell, N. I. 2009, *MNRAS*, 395, 823
- Schuh, S., Beeck, B., & Nagel, T. 2009, *Journal of Physics Conference Series*, 172, 012065
- Smith, L. F., Shara, M. M., & Moffat, A. F. J. 1996, *MNRAS*, 281, 163
- Stanghellini, L., Shaw, R. A., & Villaver, E. 2008, *ApJ*, 689, 194
- Tanner, R. W. 1948, *JRASC*, 42, 177
- Todt, H., Peña, M., Hamann, W.-R., & Gräfener, G. 2010, *A&A*, 515, A83
- Todt, H., Kniazev, A. Y., Gvaramadze, V. V., et al. 2013, *MNRAS*, 430, 2302
- Tonry, J., & Davis, M. 1979, *AJ*, 84, 1511
- Tovmassian, G. H., Napiwotzki, R., Richer, M. G., et al. 2004, *ApJ*, 616, 485
- Trumpler, R. J., & Weaver, H. F. 1953, *Dover Books on Astronomy and Space Topics*, New York: Dover Publications, —c1953,
- van der Hucht, K. A. 2001, *NAR*, 45, 135
- van Dokkum, P. G. 2001, *PASP*, 113, 1420
- van Winckel, H., Lloyd Evans, T., Briquet, M., et al. 2009, *A&A*, 505, 1221
- Werner, K., & Herwig, F. 2006, *PASP*, 118, 183
- Werner, K., Rauch, T., Reiff, E., & Kruk, J. W. 2008, *Hydrogen-Deficient Stars*, 391, 109
- Werner, K. 2012, *IAU Symposium*, 283, 196
- Zhang, X., & Jeffery, C. S. 2012, *MNRAS*, 419, 452
- Zijlstra, A. A., Gesicki, K., Walsh, J. R., et al. 2006, *MNRAS*, 369, 875

APPENDIX A: LIST OF CLOSE-BINARIES

Table A1 gives a list of published post-CE PNe updating Miszalski et al. (2011c). In the Miszalski et al. (2009a) sample, there are still some objects that require spectroscopic confirmation that the variable star identified is the CSPN. Miszalski (2009) obtained Gemini GMOS spectroscopy for several in the sample. Some objects were removed based partially on the spectra (Miszalski et al. 2011c) and several other objects were confirmed by Miszalski (2009) as true central stars (K 6-34, H 2-29, BMP 1800-3408, PPA 1759-2834, Pe 1-9, PPA 1747-3435, PHR 1757-2824, PHR 1756-3342, Sab 41, M 2-19 and M 3-16). Unpublished spectra of other objects have also been obtained, but these will be discussed elsewhere. We have removed Te 11 which is a cataclysmic variable (Drake et al. 2014) and MPA 1508-6455 which requires further work to prove its long 12.5 d period. A period of 1.26 d is adopted for PN G222.8–04.2 based on unpublished SALT RSS radial velocities from our 2013-2-RSA-005 programme.

Table A1. An updated list of 42 close binary CSPNe whose status is fairly well established.

PN G	Name	Period (days)	Discovery reference
053.8–03.0	Abell 63	0.46	Bond et al. 1978
215.6+03.6	NGC 2346	15.99	Mendez & Niemela 1981
009.6+10.5	Abell 41	0.23	Grauer & Bond 1983
055.4+16.0	Abell 46	0.47	Bond 1985
283.9+09.7	DS 1	0.36	Drilling 1985
136.3+05.5	HFG 1	0.58	Grauer et al. 1987
253.5+10.7	K 1-2	0.68	Bond & Grauer 1987
005.1–08.9	Hf 2-2	0.40	Lutz et al. 2010
017.3–21.9	Abell 65	1.00	Bond & Livio 1990
329.0+01.9	Sp 1	2.91	Bond & Livio 1990
355.2–03.6	HaTr 4	1.74	Bond & Livio 1990
144.8+65.8	BE UMa	2.29	Liebert et al. 1995
135.9+55.9	SBS 1150+599A	0.16	Tovmassian et al. 2004
341.6+13.7	NGC 6026	0.53	Hillwig et al. 2010
349.3–01.1	NGC 6337	0.17	Hillwig et al. 2010
359.1–02.3	M 3-16	0.57	Miszalski et al. 2008
357.6–03.3	H 2-29	0.24	Miszalski et al. 2008
000.2–01.9	M 2-19	0.67	Miszalski et al. 2008
005.0+03.0	Pe 1-9	0.14	Miszalski et al. 2009a
355.3–03.2	PPA 1747-3435	0.22	Miszalski et al. 2009a
355.7–03.0	H 1-33	1.13	Miszalski et al. 2009a
354.5–03.9	Sab 41	0.30	Miszalski et al. 2009a
000.6–01.3	Bl 3-15	0.27	Miszalski et al. 2009a
359.5–01.2	JaSt 66	0.27	Miszalski et al. 2009a
358.7–03.0	K 6-34	0.20	Miszalski et al. 2009a
357.0–04.4	PHR 1756-3342	0.26	Miszalski et al. 2009a
001.8–02.0	PHR 1757-2724	0.80	Miszalski et al. 2009a
001.2–02.6	PHR 1759-2915	1.10	Miszalski et al. 2009a
005.0–03.1a	MPA 1759-3007	0.50	Miszalski et al. 2009a
001.9–02.5	PPA 1759-2834	0.31	Miszalski et al. 2009a
357.1–05.3	BMP 1800-3408	0.14	Miszalski et al. 2009a
000.9–03.3	PHR 1801-2947	0.32	Miszalski et al. 2009a
222.8–04.2	PHR 0654-1045	1.26	Hajduk et al. 2010
054.2–03.4	The Necklace	1.16	Corradi et al. 2011
068.1+11.0	ETHOS 1	0.53	Miszalski et al. 2011a
049.4+02.4	Hen 2-428	0.18	Santander-García et al. 2015
034.5–06.7	NGC 6778	0.15	Miszalski et al. 2011b
338.1–08.3	NGC 6326	0.37	Miszalski et al. 2011b
290.5+07.9	Fleming 1	1.19	Boffin et al. 2012
259.1+00.9	Hen 2-11	0.61	Jones et al. 2014
086.9–03.4	Ou 5	0.36	Corradi et al. 2014
307.2–03.4	NGC 5189	4.04	This work

**APPENDIX B: LOG OF
CROSS-CORRELATION RESULTS**

Table B1. Log of cross-correlation wavelength ranges, RV shifts, errors and XCSAO cross-correlation peak heights h .

Object	λ range (Å)	Grating	MJD (mid) (Days)	v_i (km s ^{−1})	Δv_i (km s ^{−1})	h	
Hen2-113	4477–4705	4	56063.812846	−59.7	4.9	0.97	
			56063.823819	−60.0	4.8	0.97	
			56063.836879	−60.1	4.7	0.97	
			56063.869755	−60.3	4.5	0.98	
			56064.122231	−56.0	4.0	0.97	
			56064.801191	−59.0	5.0	0.97	
	5050–5500		56063.812846	−61.4	7.0	0.81	
			56063.823819	−60.0	6.0	0.82	
			56063.836879	−63.0	6.0	0.89	
			56063.869755	−60.0	6.0	0.92	
			56064.122231	−61.1	7.2	0.90	
			56064.801191	−52.9	7.0	0.74	
	5050–5500	6	56069.996481	−50.5	5.0	0.97	
			56106.823001	−60.1	4.9	0.98	
			56108.917004	−64.9	6.6	0.92	
			56108.928125	−58.2	5.6	0.91	
			56109.813025	−68.5	5.7	0.89	
			56111.030991	−56.2	4.9	0.98	
Hen3-1333	4500–4720	6	56106.927875	−41.8	4.4	0.98	
			56108.109317	−40.2	4.4	0.98	
			56109.996351	−48.2	4.7	0.98	
			56111.057141	−47.3	4.3	0.99	
			4785–5420	56106.927875	−44.8	4.1	0.98
				56108.098274	−47.4	13.0	0.58
	56108.109317	−35.0		4.3	0.98		
	56109.996351	−47.1		4.1	0.98		
	56111.057141	−49.1		4.6	0.97		
	6000–6288	56108.899327		−45.0	4.0	0.98	
		56109.131929	−35.0	5.3	0.98		
		56109.873401	−45.1	3.9	0.98		
		6734–7057	56108.899327	−40.5	3.9	0.98	
			56109.131929	−41.2	4.3	0.98	
			56109.873401	−45.1	3.9	0.98	
	Hen2-99	4500–5740	6	56107.745127	−35.6	13.7	0.98
				56068.820887	−59.0	12.7	0.98
				56110.976449	−56.0	14.3	0.98
56111.821737				−54.5	12.6	0.98	
56106.744197				−44.5	15.0	0.97	
6630–7300		56108.866659	−62.0	14.1	0.96		
		56109.747499	−75.5	16.2	0.96		
		6000–6490	56108.866659	−58.6	15.0	0.87	

Table B2. Table B1 (continued).

Object	λ range (Å)	Grating	MJD (mid) (Days)	v_i (km s ^{−1})	Δv_i (km s ^{−1})	h
NGC 5315	4477–4705	6	56068.848701	93.9	6.5	0.76
			56106.777051	95.8	11.5	0.83
			56110.773799	65.8	6.1	0.82
	5050–5500		56109.782759	79.7	6.4	0.96
PMR 2	4477–5400	6	56107.709237	2.1	6.4	0.98
			56110.721211	4.6	12.0	0.80
			56110.735899	−1.3	6.2	0.98
	6321–6536		56106.715497	0.4	6.1	0.98
			56108.713129	9.5	6.4	0.96
			56109.713509	9.7	8.5	0.94
			56109.843839	10.0	8.4	0.84
NGC 5189	5169–5443	PG 2300	56672.581101	−34.6	6.0	0.90
			56674.596367	36.1	7.9	0.85
			56677.556460	56.7	6.0	0.86
			56685.583323	61.6	5.9	0.85
			56698.625846	70.3	5.5	0.85
			56700.550927	−40.4	5.6	0.87
			56701.611668	51.6	4.4	0.90
			56704.578300	−37.0	6.8	0.88
			56705.486876	49.4	3.7	0.88
			56705.506708	44.1	6.1	0.83
			56706.566535	57.6	5.1	0.87
			56707.556766	−14.9	4.9	0.91
			56731.589104	20.8	4.7	0.85
			56733.414920	4.2	3.7	0.90